



UCRL-ID-123392

PCMDI Report No. 31

**SEASONAL CHARACTERISTICS OF PRECIPITATION
OVER THE UNITED STATES IN AMIP SIMULATIONS**

by

James S. Boyle

Program for Climate Model Diagnosis and Intercomparison
Lawrence Livermore National Laboratory, Livermore, CA, USA

February 1996

**PROGRAM FOR CLIMATE MODEL DIAGNOSIS AND INTERCOMPARISON
UNIVERSITY OF CALIFORNIA, LAWRENCE LIVERMORE NATIONAL LABORATORY
LIVERMORE, CA 94550**

DISCLAIMER

This document was prepared as an account of work sponsored by an agency of the United States Government. Neither the United States Government nor the University of California nor any of their employees, makes any warranty, express or implied, or assumes any legal liability or responsibility for the accuracy, completeness, or usefulness of any information, apparatus, product, or process disclosed, or represents that its use would not infringe privately owned rights. Reference herein to any specific commercial product, process, or service by trade name, trademark, manufacturer, or otherwise, does not necessarily constitute or imply its endorsement, recommendation, or favoring by the United States Government or the University of California. The views and opinions of authors expressed herein do not necessarily state or reflect those of the United States Government or the University of California, and shall not be used for advertising or product endorsement purposes.

This is an informal report intended primarily for internal or limited external distribution. The opinions and conclusions stated are those of the author and may or may not be those of the Laboratory.

This report has been reproduced
directly from the best available copy.

Available to DOE and DOE contractors from the
Office of Scientific and Technical Information
P.O. Box 62, Oak Ridge, TN 37831
Prices available from (615) 576-8401, FTS 626-8401

Available to the public from the
National Technical Information Service
U.S. Department of Commerce
5285 Port Royal Rd.,
Springfield, VA 22161

Abstract

The monthly mean precipitation patterns of the Atmospheric Model Intercomparison Project (AMIP) decadal simulations over the US and adjoining oceans are intercompared. A simple harmonic analysis of the 12 month seasonal mean precipitation values and a principal component(PC) analysis of the 120 monthly values were carried out. Emphasis is placed on the basic seasonal variation for three sub-regions, the Eastern US, Central US and West Coast US.

The results indicate the following: (1) There are rather severe problems for almost all the models in capturing the seasonal variation of the precipitation over the Eastern US. The models typically overemphasize the Summer / Spring rainfall amounts. The PC analysis indicates that many of the models tend to extend the precipitation regime typical of the Central US too far to the east, resulting in a precipitation maxima occurring in the summer for the Eastern region. (2) The seasonal variation of the west coast is handled with the greatest fidelity. This result cuts across all the models and may be attributable to the fact the SST forcing is specified and common to all the simulations. The common SST forcing is apparently a dominant factor in determining this region's precipitation climatology. (3) On the space scales of the regions selected, there is little consistent evidence that points to any specific model feature as a predictor of model performance. None of the obvious candidates such as horizontal resolution, convective closure schemes or land surface schemes are reliable discriminators of a model's ability to simulate precipitation. (4) For one smaller sub-region centered over Arizona, chosen because of the dominance of the semianual cycle, there is evidence that increased horizontal resolution has an effect. For this intermountain region the higher resolution models as a whole do better than the low resolution models. However, even in this case there is enough variation amongst the individual simulations as to obscure the conclusion that increased horizontal resolution is a necessary or sufficient quality to produce a reliable simulation. (5) The models tend to have less interannual variation than the observations with more variance being explained by the leading (annual cycle) PC, while the observations have a less peaked spectrum. (6) The models consistently overestimate the precipitation in the spring and early summer in all regions. This might indicate a common failing of all the convective schemes in dealing with extratropical convective instability that is endemic to this time of year.

It would appear that the models of the generation represented by the AMIP integrations would not be suitable for direct coupling to a watershed disaggregation scheme even on a seasonal basis. The results indicate that there is substantial uncertainty in the distribution of precipitation throughout the year as simulated by most of these models.

1. Introduction

The seasonal precipitation patterns across the United States represent a broad range of climate types indicative of diverse precipitation mechanisms. These patterns have been documented in many works, e.g. Hsu and Wallace(1976), Horn and Bryson(1960), Kirkyla and Hameed(1989). It is challenge for a climate general circulation model (GCM) to produce precipitation patterns that match those observed over the US. In order to be successful the model must be capable of simulating the proper interaction of a number of precipitation producing phenomena such as synoptic scale storms, convective complexes, upslope enhancement, and even some tropical systems.

Hsu and Wallace (1976), applying a harmonic analysis to 30 years of precipitation observations over the continental US, established that there were the following regimes:

- (a) An area of pronounced winter maximum in the western states with a Mediterranean regime to the south and west coast regime in the Pacific northwest.
- (b) A broad flat area of early summer maxima over the great plains and Great Lakes, a continental interior regime.
- (c) Small areas of late summer maxima over Florida and west Texas which are probably monsoonal in character.
- (d) A region of weak spring maxima over the interior of the southeastern states.
- (e) A region of weak seasonal variability over the middle and north Atlantic states.
- (f) A region of strong semi-annual variability with February and August maxima, centered over Arizona.

These patterns are a result of a subtle blending of a number of physical processes and geographical characteristics. The geographical detail of the above climate regimes should not be expected to be simulated by some of the coarser grid models. The ability of a model to properly simulate the annual cycle of precipitation would appear to be a necessary precursor to making predictions based on various climate change scenarios. In addition, the value of climate predictions to watershed variability depend on an accurate annual cycle. If the precipitation is not distributed correctly through the year then the predictions are not as useful for agricultural or hydrological purposes.

In this work the results of all 30 AMIP models will be intercompared with an observed data set. The focus will be on evaluating the annual cycle of precipitation on space scales consistent with the capabilities of all the models. The next section will describe the data sets used and the analysis procedures. The analyses are simple and straightforward: harmonic decomposition, principal component analysis, and statistics from a multiple random block permutation of monthly mean data. Section three presents the results and section four discusses some ramifications of the results.

2. Data and data procedures

a. Data sets

The Atmospheric Model Intercomparison Project (AMIP) of the World Climate Research Programme's Working Group on Numerical Experimentation (WGNE) provides a rich data set for model intercomparison. The participants in AMIP simulated the global atmosphere for the decade 1979 to 1988 using a common solar constant and CO₂ concentration, and a common monthly averaged SST and sea ice data set. An overview of AMIP is provided by Gates (1992).

The AMIP models used in this study are identified in Table 1 (taken from Phillips, 1994) and their horizontal and vertical resolutions are shown. As important as the spatial configuration of the model are the parameterizations used to simulate moist convective heating, fluxes of heat, moisture and momentum, precipitation, clouds and so forth. The complete specifications of the parameterizations used in the models are described in Phillips (1994). The penetrative convective parameterization is a crucial element in the simulated precipitation but it is difficult to succinctly characterize such schemes. For a specific scheme, say that of Kuo, there are so many variations and critical differences in implementations that simply identifying a parameterization by a single nomenclature can be misleading.

The observed data used here were blended from two sources. Over the land the data were from Schemm et al. (1992). These data were derived from station data and gridded to a 4 x 5 latitude, longitude mesh. Over the ocean the data were from the MSU estimates of Spencer (1993). These observations are taken over the same time period as the AMIP simulations (1979 to 1988) and consist of monthly mean data.

For the models participating in AMIP there are available monthly means of precipitation (120 months of data) on the native grid of the model. This is a gaussian

grid for the spectral models and usually a regular latitude, longitude grid for the grid-point models. Monthly data for individual years were averaged together to obtain means for the 12 months of the year.

This study also makes use of four additional AMIP simulations of the ECMWF model. The five ECMWF integrations used identical boundary forcings as specified in the AMIP but differed in the initial conditions used. The initial run (the original AMIP entry) used the observed fields to start the model on 1 January 1979. Subsequent runs used the endpoints of the previous simulation as their initial data. This ensemble of five integrations is used to provide some indication of the extent of the intrinsic variability that might be expected for a single model. This provides a useful perspective when comparing the results of the single integration of a number of models.

b. Harmonic analysis

The 12 monthly mean of each data set were subjected to harmonic analysis, which yielded the amplitudes and phases of the first and second harmonics of the annual cycle. The initial interest is in how much the annual and semiannual cycles modulated the rainfall in various regions without regard to the annual mean precipitation. Thus, normalized rather than raw amplitudes will be displayed on the phase/amplitude diagrams. Normalized amplitudes are obtained by dividing the raw amplitudes obtained from the harmonic analysis by the average monthly precipitation, as in Hsu and Wallace (1976). The harmonic analysis was carried out on a point by point basis and was performed on the native grid of each model.

c. Principal component analysis

A principal component (PC) analysis was carried out using a 4 x 5 degree latitude longitude grid centered on the US identical to that of the observed data set. The grid consisted of 95 gridpoints as shown in Fig. 1. The covariance matrix for input into the principal component routines consisted of 120 time points at the 95 points of the grid. The 120 month average was removed at each grid point for these analyses. This removes the bias but retains the trend and seasonal cycle. The PC analysis used the PRIN algorithm of IMSL (1995).

d. Multivariate random block permutation procedure

Tucker et al. (1989) describe a procedure for verifying numerical models using a multivariate randomized block permutation procedure (MRBP). Such methods require relatively few data to establish meaningful comparisons and also make minimal assumptions as to the independence of the samples. The strong correlations in time and space of meteorological data make the estimates of effective degrees of freedom in more traditional statistics rather difficult.

The MRBP procedure was applied on pairs comprising the models (re-gridded to the 4 x 5 grid of 95 points) and the observations for the 12 month mean annual cycle of each. In the nomenclature of the test there were 2 blocks (observed, model), 12 groups or treatments, and 95 measurements or responses. The results will be presented by two numbers, ρ which is a measure of agreement between data sets and P which is the probability that the results obtained could have been produced by chance. ρ varies from 0 to 1, with the low value indicating no agreement and, the high value indicating perfect agreement. As a basis for comparison the MRBPP was also computed for 5 ensembles of the ECMWF model. In this case there are 5 blocks of 12 groups at 95 points.

3. Results

a. Harmonic analysis

Figure 1 is a chart of the normalized amplitude and phase of the annual cycle in precipitation over the US using the observed data set described above. Figure 1 compares well with the analogous chart of Hsu and Wallace (1976), their Fig. 8. The data of Hsu and Wallace have more detail than Fig. 1 since they used the individual stations which have a fairly dense distribution over the US. However, since our purpose is to compare against GCM output, Fig. 1 is depicting the level of detail appropriate for many of the models participating in AMIP (see Table 1). From the discussion in Hsu and Wallace (1976), it appears reasonable to distinguish three large-scale regimes for the annual cycle over the continental US: A western region, 130W-110W, 30N-50N, which has a winter maximum; a central region, 110W-90W, 30N-50N, with a summer maximum; and an eastern region, 90W-75W, 30N-45N, with a relatively weak annual cycle. One might argue over the individual merits of data sets and anal-

ysis techniques, but a rough division into these three regions would appear to be robust across all data sets. From a practical standpoint, since there are so many models to be intercompared, we must simplify the analysis to a few manageable points of comparison. A presentation of all the model results as in Fig. 1 would be overwhelming. Figure 2 presents curves of the observed data set averaged over the regions described above for the 12 months of the year. Subsequent presentations of the models will be deviations from these observed averages. The precipitation is averaged over the area indicated from the native grid of the models. These data represent means over ten seasonal cycles and as such should be fairly robust indicators of the model climate. Hsu and Wallace (1976) indicate that five to six years of data are sufficient to characterize the seasonal cycle from observed data.

Figure 3a presents the deviations between the observations and the models for the annual cycle in precipitation over the eastern region of the US, 90W-75W, 30N-45N. The dark shading indicates a model is overestimating the precipitation, the light shading indicates that the model is too dry. The most general observation from Fig. 3a is that the models tend to have a distinct spring or summer surplus and a fall and winter deficit, although there is a considerable amount of variation. This pattern is a consequence of the fact that most of the models have a substantially greater seasonal variation than the observations with a distinct spring/summer maximum and a winter minimum. There are some models that have a relatively subdued seasonal cycle, but virtually all the models have more variation than the observations. As will be shown, this apparent superiority of some models is often the result of compensating errors in the region rather than an overall superior simulation.

Figure 3b shows the annual cycle in precipitation for the central US region. Note the presence of a distinct summer maximum and winter minimum in the observed data on the top of the plot. The models tend to capture this seasonal variation but often have much too large an amplitude. There is also a tendency to push the maximum to occur too early in the spring. The models in general overestimate the precipitation in this region, especially in the spring and summer.

Figure 3c shows the annual cycle in precipitation for the western US region. There is an improvement from the previous two figures in that overall the models have smaller deviations. Once again there is a tendency to overestimate the springtime amounts. The summertime minima appears to be more faithfully simulated than the magnitude of the winter maximum in this region. This could be the result of using

common SSTs, so that all the models are driven by the same cold water off the west coast that suppresses summer rainfall. It is rather remarkable that although the observed climatological phase is reversed in going from the central to the western region, the nature of the deviations between Figs. 3b and 3c are quite similar. The spring and early summer regimes are obviously difficult periods for the models to simulate across the whole US.

The deviations of Fig. 3 are not related in any obvious way to a single property of the model formulation. A model with low resolution such as GISS #11 appears to perform better than models with more than double the number of gridpoints. Neither is the type of convective parameterization a robust discriminator. The GLA model (#12), has somewhat different values in Fig. 3 than UCLA (#26) but both have the same horizontal resolution and both use a version of the Arakawa-Schubert convective scheme. However, an almost all-pervasive characteristic is an overestimate of precipitation in the spring and early summer. This might indicate a shortcoming in the formulation of almost all the convective parameterizations in dealing with mid-latitude convective instability endemic to this season. It is possible that parameterizations that are optimized for tropical convection do not perform as well in the midlatitude convective regimes. In the next section an attempt will be made to relate the patterns seen in Fig. 3 to individual phase/amplitude diagrams of the models. A few models will be drawn out to make particular points, but this should not be construed as judging these models as either overall superior or inferior to the others.

In Fig. 3 models #18(MPI) and #11(GISS) have distributions of precipitation through the year that match the observations fairly well, and that match each other. Figure 4a,b displays the normalized amplitudes and phase for these models in the same format as Fig. 1 (the observations). The MPI was run at a spectral resolution of T42. The points on Fig. 4a reflect the gaussian grid for this resolution which is approximately 2.5×2.5 degrees. The GISS model ran on a 4×5 grid. It can be seen that in the eastern region for both models there is a stronger seasonal variation than in the observations (i. e. larger arrows). The profile for the twelve months tends to be flat because the various components over the region have compensating phases that flatten out the average amplitude. This is in contrast to the observations, Fig. 1, which have relatively small arrows throughout the region. This type of behavior occurs commonly in the models that display a small seasonal amplitude in the eastern region. The MPI model has strong compensation in the north / south direction while the GISS

model has a more subtle phase shift in the east / west direction.

Figures 4c and 4d present an interesting pair of models, namely the JMA and NCAR CCM2, respectively. Both are T42 resolution and in Figs. 3a and 3b they have substantial deviations of almost opposite sign. There is a dramatic phase difference between the two models over the eastern region. The JMA model also does quite poorly in the central US, strongly underestimating the summer maximum.

The CSU model was the only model to miss the phase in the western region, as shown in Fig. 4e. The CSU model was of coarse resolution (4×5), and apparently extended the summer maximum regime of the central region too far to the west. This is not solely due to the resolution since the GISS model, and all other 4×5 models, do not suffer this fate. The UCLA model, a close cousin to the CSU model, does display a tendency similar to CSU although not as extreme.

The final figure of this set is Fig. 4f for the RPN model. This model has the highest horizontal resolution of all the models considered. This model also has problems in that there is too much seasonal variation in the eastern region. What is important is the pleasing transition as one passes from the Great Plains across the Rockies and Sierras to the west coast. Although this particular model may not be perfect, the ability to capture the details in these transition regions is clearly a desirable feature of the models.

b. *Semi-annual patterns*

Figure 5 displays the semi-annual phase/amplitude plot for the observations. The gridpoints where the semiannual cycle exceeds the annual are indicated by the large filled circles. This figure can be compared to the corresponding figure from Hsu and Wallace (1976), their Fig. 9. The most prominent region discussed by Hsu and Wallace (1976) is the area of the southwestern "monsoon" located over Arizona. The extent of the regions where the semiannual cycle dominates are generally limited in area. Even among the various observed data sets that were used in this work there was not a strong consensus on the regions where the semi-annual cycle is strongest. Probably the most consistent and prominent semi-annual feature amongst the observed data is in the southwestern monsoonal region.

Figure 6 is the same as Fig. 3 except for the region (29N-36N, 111W-102W) centered over Arizona. The ability to simulate precipitation over this region varies widely

among the models. As with the larger regions used in Fig. 3, it is not completely fair to compare these global models over such small areas. The original formulation of the models was not intended to simulate small scale detail, and a shift in just a few degrees of the averaging region can alter an individual result dramatically. One other important difference in Fig. 6 and Fig. 3, is that in Fig. 6 the models have been sorted by horizontal resolution. To keep things simple the criterion for the sort was just the number of north/south nodes of the grid used for the physical parameterizations. The coarsest (4×5 , 45 latitude nodes) models start with #1. Two interesting transition points are at model #17 which starts the T42 (64 latitude nodes) models and model #26 which starts those above T42 resolution. The figure graphically shows that for this small, mountainous region higher resolution is definitely an aid to a better simulation. Also obvious is that higher resolution is neither necessary nor sufficient to produce a superior simulation by this measure. There are models of coarser resolution which outperform those of finer grids. As described by Hales (1974), the precipitation in this region is driven by the moisture influx from the Sea of Cortez and the Gulf of Mexico, as well as from the Pacific. The models must properly handle the moisture from these sources and the resulting convective instability over elevated terrain and channel it through the mountains. This is a stiff test for any GCM, but one that will have to be addressed as climate change issues are brought to the local watersheds.

c. *Principal component analyses*

Principal components analyses are a powerful method of summarizing data. Figure 7 shows time series of the leading two principal components (PC) for the observations and the models. It is obviously not the intent of these figures to track the time evolution of any particular model but to yield an overall impression of their relative behavior. The dominance of the seasonal cycle is seen in Fig. 7a, the leading PC. Although the phase agreement is good among the models and the observations, there is quite a variation in amplitude. The models tend to have less interannual variation than the observations and a larger amplitude. In the second component, Fig. 7b, agreement in phase is non-existent.

Figure 8 is a bar chart of the percent variance explained by the leading three PCs for the AMIP models and observations. All the models, save two, have a greater percentage in the leading (pre-dominantly seasonal) component. The models tend to have a more regular seasonal cycle that produces a steep PC spectrum, with the lead-

ing component rather more heavily loaded compared to the observations.

Figure 9 is the leading principal vector of the observed precipitation data. Comparing Fig. 1 and Fig. 9 one can clearly see the distinct seasonal climate regimes. The west coast has an opposite phase to the central US, and zero lines run through the inter-mountain region and down the east coast. The zero contour identifies regions which tend to have a small seasonal cycle and where the semi-annual cycle might dominate. In the next section, the leading principal vectors of the same models that were used to present the phase amplitude diagrams in Fig. 4 will be shown. As seen by the observed fields in Fig. 1 and Fig. 9 the leading PC allows for a succinct, scalar characterization of the seasonal cycle of precipitation.

Figure 10a shows the leading principal vector for the GISS model. This model has a relatively small difference from the observations, although the eastern region is still a problem. Figure 10b shows the MPI model. This plot makes clear the north south dipole over the eastern US which is quite different from the observations.

Figure 10c is the leading PC projection for the NCAR (CCM2) model. The central summertime convective regime is located too far eastward, which results in a large seasonal cycle with a summer maximum, as seen in Figs. 3a and 3b. This illustrates a problem common to many of the models. Figure 10d shows a less common problem displayed by the JMA model in which the model's eastern Atlantic coastal climate regime extends too far to the west. This results in errors of opposite sign to the NCAR model in Fig. 3a and 3b. Figure 10e for the CSU model vividly illustrates the dramatic difference with the observations that this model displays. The fine resolution of the RPN model, Fig. 10f, is not a panacea. This model also illustrates an anomalously large variation over northern Mexico, a trait which is shared with many of the other models.

The final two figures in this series, Figs. 10g and 10h, are the ECMWF and UGAMP models, respectively. These models, along with the MPI model, form an interesting trio. All three share a close common formulation and resolution and the ECMWF and UGAMP models are almost identical except for their convective schemes. The ECMWF model uses the Tiedtke mass flux parameterization whilst the UGAMP model uses the Betts-Miller convective adjustment formulation. Although the MPI model has the same convective scheme as the ECMWF, it has numerous other differences from its progenitor. In comparing Figs. 10g and 10h, one is essentially comparing the results from two convective schemes for the same model. It appears from this

comparison that the convective scheme has an impact that is larger than that induced by the modifications of the MPI model from the ECMWF. This comparison also shows that just a difference in convective scheme can establish a difference between model, and shows that other differences in model formulation can easily obscure the distinctions due to convective schemes.

d. Multivariate random block permutation procedure

In order to place the results of the MRBP statistics in perspective, the MRBP procedure was run on the five ensembles of the ECMWF model. In this case the number of blocks was five and the value of ρ was 0.6 and P was 10^{-29} . Thus there is a virtually certainty, by this test, that the results are not due to chance. Note that ρ is not 1 in this case, even with the same model as there is variation in the seasonal cycle of the precipitation fields. This result indicates that one cannot reasonably expect to have a ρ value close to one when comparing a single integration to the observations.

The results for the full AMIP suite is presented in Table 2. The values of ρ range from 0.1 to 0.25. This is not a very encouraging result even in light of the ensemble calculations. One should expect a decrease from the ensemble values, but not by a factor of three. The probability of these values occurring by chance is low for most of the models, although in the worse cases is not completely negligible as it approaches the 5% level. The range in ρ values for the 5 ECMWF ensembles each taken pairwise with the observations was 0.02 with the values ranging from 0.21 to 0.19. To be conservative, model single integrations that have ρ values that differ by less than this value should not be distinguished. It is rather sobering to realize that this analysis has been carried out on the seasonal cycle of the simulations, and that at this basic level of comparison the models do not do well.

4. Discussion and conclusion

A principal objective of AMIP was to be able to analyze the factors that contributed to model differences and error. Over the US there are a number of model specific differences that could account for variations in the simulated precipitation fields, such as horizontal and vertical resolution (varying representation of topography), convective parameterization, cloud parameterization, land-surface processes etc.

The MRBP results are a single number and as such can provide a simple basis

for comparison. The best result for the MRBPP came for the RPN model. This is the model with the highest horizontal resolution. The next best model by this measure is the UKMO model which also has relatively good horizontal resolution. However, the COLA model which has comparable resolution to RPN is far down on the list, below even those models with substantially less horizontal resolution. A number of models have a spectral resolution of T42 (ECMWF, MPI, CCM2, NMC, NRL, UGAMP, CN-RM, DERF and JMA). These models of identical resolution just about span the range of the ρ values, although there is a slight tendency to be at the high end. This indicates that at least by this measure, horizontal resolution is not the sole arbiter of model performance. As one goes down the list of other possible classifications by formulation, similar results obtain. This conclusion is also supported by Fig. 3, in which the magnitude of the deviations from observations cannot be attributed to any specific model characteristic.

The conclusion is that the models represented by AMIP are severely deficient as to the proper description of precipitation over the US. It should be realized that the performance of these models is by no means uniform, as some perform somewhat better than others. It might well be that models that do well in this rather restricted region might have problems in other areas of the globe and vice-versa. Finally, the AMIP models are by now obsolete, as virtually every modeling group has improved their models after these integrations; it will be of interest to ascertain how well the new models fare.

Acknowledgments. The cooperation of the ECMWF in making their forecast model available and in providing expert technical advice for this research is gratefully acknowledged. The generosity of the modeling groups involved in AMIP in making their results available is greatly appreciated. Dr. Paul Mielke, Jr. generously supplied the code for computing the MRBP statistics. This work was performed under the auspices of the Department of Energy Environmental Sciences Division by the Lawrence Livermore National Laboratory under contract W-7405-ENG-48.

References

- Flury, B., 1988: *Common Principal Components and Related Multivariate Models*, J. Wiley, New York, pp 258.
- Frankigoul, C., S. Fevrier, N. Sennechael, J. Verbeek, and P. Braconnot, 1995: An intercomparison between four tropical ocean models: Thermocline variability. *Tellus*, **47A**, 351-364.
- Gates, W. L., 1992: AMIP : The atmospheric model intercomparison project. *Bull. Amer. Meteor. Soc.*, **73**, 1962-1970.
- Hales, J. E., 1974: Southwestern United States summer monsoon source Gulf of Mexico or Pacific Ocean. *J. Appl. Meteor.*, **13**, 331-342.
- Horn, L. H. and R. A. Bryson, 1960: Harmonic analysis of the annual march of precipitation over the United States. *Ann. Assoc. Amer. Geogr.*, **50**, 157-171.
- Hsu, C.-P. and J. M. Wallace, 1976: The global distribution of the annual and semi-annual cycles in precipitation. *Mon. Wea. Rev.*, **104**, 1093-1101.
- IMSL Stat/Library, 1991: IMSL Inc., Houston, 1578pp.
- Kirkyla, K. I. and S. Hameed, 1989: Harmonic analysis of the seasonal cycle in precipitation over the United States: a comparison between observations and a general circulation model. *J. Clim.*, **2**, 1463-1475.
- Phillips, T. J., 1994: A summary documentation of the AMIP models. PCMDI Report No. 18, Program for Climate Model Diagnosis and Intercomparison, University of California, Lawrence Livermore National Laboratory, Livermore, CA, 343pp.
- Schemm, J. S., S. Schubert, J. Terry, and S. Bloom, 1992: Estimates of monthly mean soil moisture for 1979-1989. NASA Technical Memorandum 104571; 254pp
- Spencer, R. W., 1993: Global oceanic precipitation from the MSU during 1979-91 and comparisions to other climatologies. *J. Clim.*, **6**, 1301-1326.
- Tucker, D. F., P. W. Mielke, Jr., and E. R. Reiter, 1989: The verification of numerical models with multivariate randomized block permutation procedures. *Meteorol. Atmos. Phys.*, **40**, 181-188.

Table 1: Model representation/resolution. The table lists the horizontal representation and resolution, the vertical coordinates and number of prognostic vertical levels (number below 800 hPa, above 200 hPa) and the atmospheric bottom and top pressure levels(for a surface pressure of 1000 hPa) From Phillips (1994).

AMIP Model	Horizontal		Vertical		
	Representation	Resolution	Coordinates	No. Levels	Bottom, Top
BMRC	spectral	rhomboidal 31	sigma	9 (3, 3)	991, 9 hPa
CCC	spectral	triangular 32	hybrid	10 (3, 4)	980, 5 hPa
CNRM	spectral	triangular 42	hybrid	30 (4, 20)	995, 0.01 hPa
COLA	spectral	rhomboidal 40	sigma	18 (5, 4)	995, 10 hPa
CSIRO	spectral	rhomboidal 21	sigma	9 (3, 3)	979, 21 hPa
CSU	finite difference	4 x 5 degrees	modified sigma	17 (2, 6)	variable, 51 hPa
DERF	spectral	triangular 42	sigma	18 (5, 5)	998, 2 hPa
DNM	finite difference	4 x 5 degrees	sigma	7 (1, 1)	929, 71 hPa
ECMWF	spectral	triangular 42	hybrid	19 (5, 7)	996, 10 hPa
GFDL	spectral	rhomboidal 30	sigma	14 (4, 4)	997, 15 hPa
GISS	finite difference	4 x 5 degrees	sigma	9 (2, 2)	975, 10 hPa
GLA	finite difference	4 x 5 degrees	sigma	17 (5, 4)	994, 12 hPa
GSFC	finite difference	4 x 5 degrees	sigma	20 (5, 7)	994, 10 hPa
IAP	finite difference	4 x 5 degrees	modified sigma	2 (0, 0)	800, 200 hPa
JMA	spectral	triangular 42	hybrid	21 (6, 7)	995, 10 hPa
LMD	finite difference	50 sinlat x 64 lon	sigma	11 (3, 2)	979, 4 hPa
MGO	spectral	triangular 30	sigma	14 (5, 4)	992, 13 hPa
MPI	spectral	triangular 42	hybrid	19 (5, 7)	996, 10 hPa
MRI	finite difference	4 x 5 degrees	hybrid	15 (1, 9)	variable, 1 hPa
NCAR	spectral	triangular 42	hybrid	18 (4, 7)	992, 3 hPa
NMC	spectral	triangular 40	sigma	18 (5, 4)	995, 21 hPa
NRL	spectral	triangular 47	hybrid	18 (5, 5)	995, 1 hPa
RPN	spectral semi-Lagrangian	triangular 63	sigma	23 (7, 7)	1000, 10 hPa
SUNYA	spectral	rhomboidal 15	sigma	12 (3, 5)	991, 9 hPa
SUNYA/NCAR	spectral	triangular 31	hybrid/sigma	18 (4, 7)	993, 5 hPa
UCLA	spectral	4 x 5 degrees	modified sigma	15 (2, 9)	variable, 1 hPa
UGAMP	spectral	triangular 42	hybrid	19 (5, 7)	996, 10 hPa
UIUC	finite difference	4 x 5 degrees	sigma	7 (3, 0)	990, 200 hPa
UKMO	finite difference	2.5 x 3.75 degrees	hybrid	19 (4, 7)	997, 5 hPa
YONU	finite difference	4 x 5 degrees	modified sigma	5 (1, 1)	900, 100 hPa

Table 2. Multivariate randomized block permutation procedure results comparing the observed seasonal cycle of precipitation over the US to the model simulations.

model	p	P	model	p	P	model	p	P
BMRC	0.17	.002	GISS	0.23	.001	NMC	0.21	.001
CCC	0.20	.001	GLA	0.18	.002	NRL	0.15	.020
CNRM	0.11	.470	GSFC	.018	.002	RPN	0.25	.000
COLA	0.18	.012	IAP	0.11	.099	SUNY	0.16	.002
CSIRO	0.17	.004	JMA	0.21	.001	SUNY/G	0.20	.004
CSU	0.12	.022	LMD	0.18	.002	UCLA	0.15	.004
DERF	0.19	.001	MGO	0.13	.008	UGAMP	0.24	.000
DNM	0.10	.067	MPI	0.18	.002	UIUC	0.14	.012
ECMWF	0.20	.001	MRI	0.18	.002	UKMO	0.24	.002
GFDL	0.18	0.14	NCAR	0.20	.003	YONU	0.11	.001

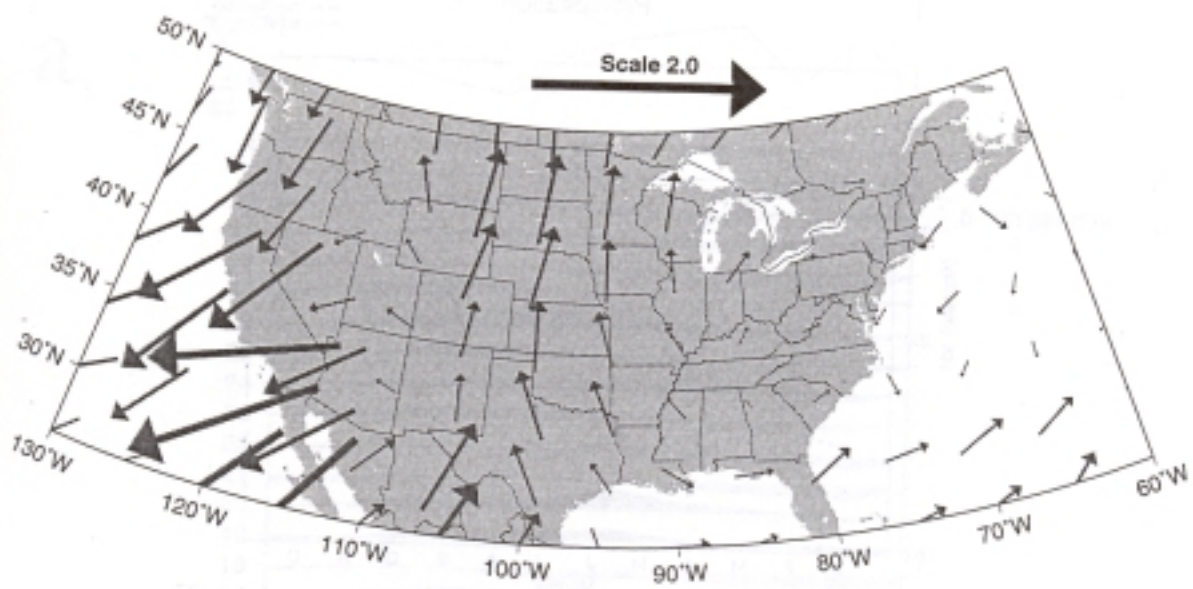


Figure 1. Normalized amplitude and phase of the annual cycle in precipitation over the United States from the observed data set described in the text. Normalized amplitude is indicated by the length of the arrows. Phase is indicated by the orientation of the arrows. An arrow pointing from north to south indicates a maximum on 1 January, one pointing from the east indicates a maximum on 1 April, etc. The arrow on the top provides the scale for a normalized amplitude equal to 2.0.

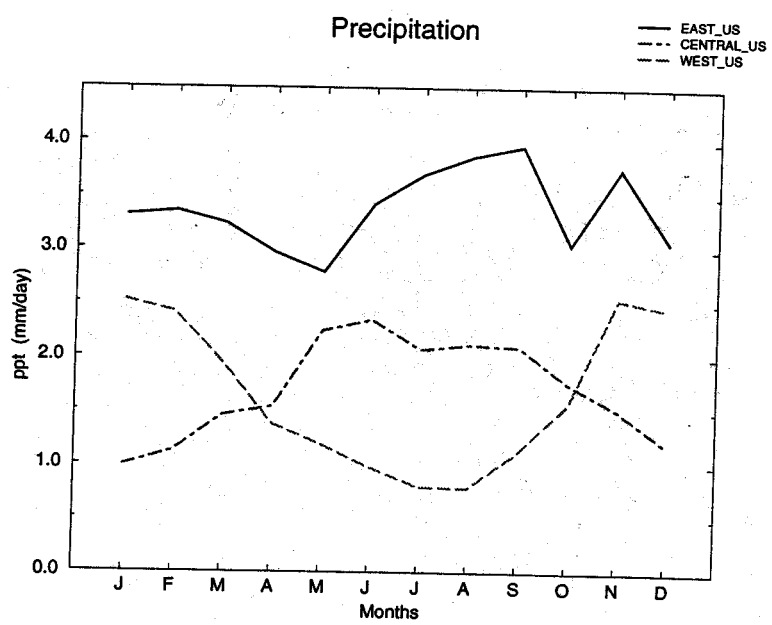


Figure 2. Areal averaged seasonal distribution of precipitation for three regions, eastern US ($30-45^{\circ}\text{N}$, $90-75^{\circ}\text{W}$), central US ($30-50^{\circ}\text{N}$, $110-90^{\circ}\text{W}$), western US ($30-50^{\circ}\text{N}$, $130-110^{\circ}\text{W}$) using the observed data set described in the text.

a

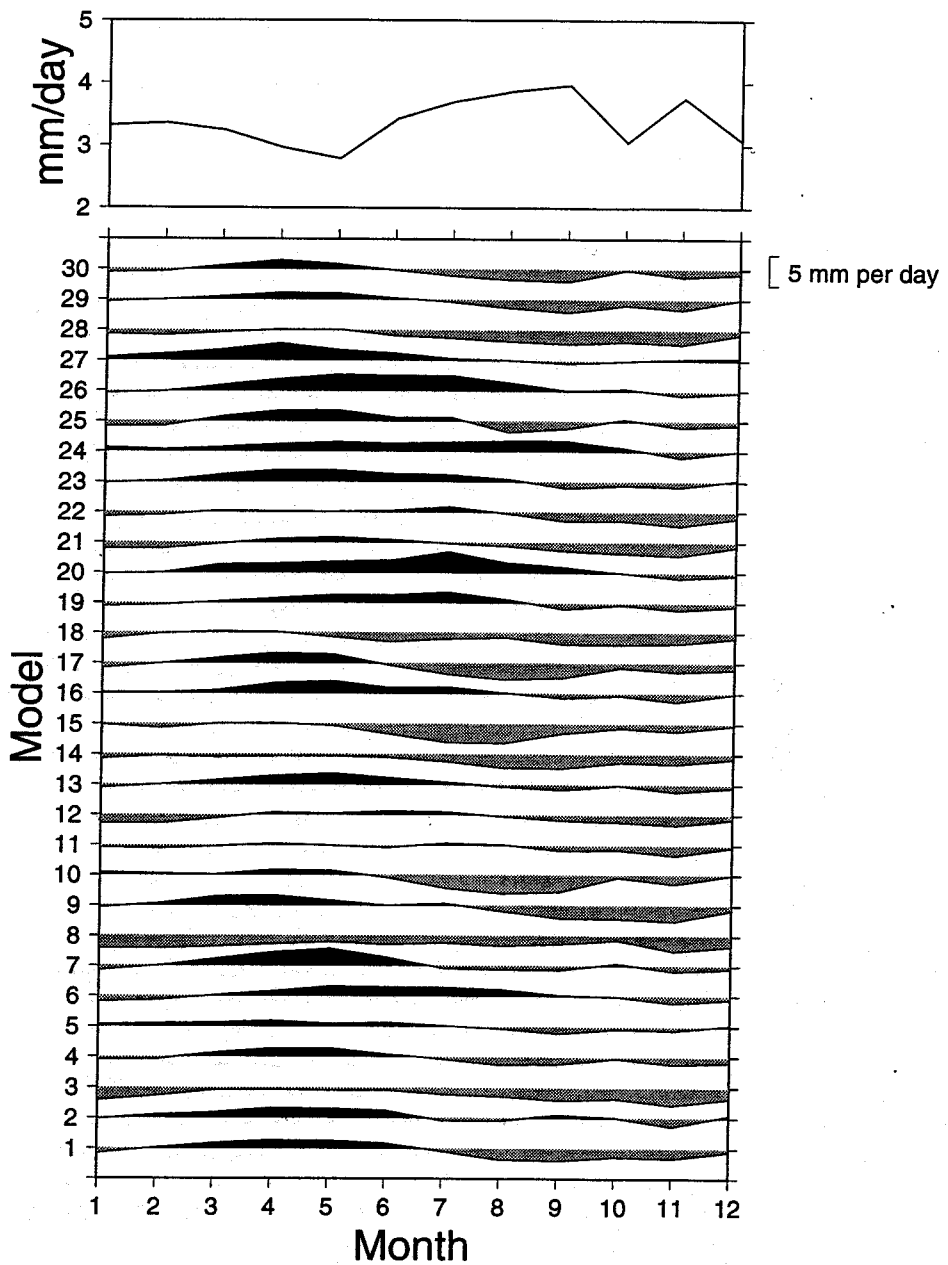


Figure 3. Deviations of the areal averaged precipitation of the AMIP models from the observations over the 10 year (1979 to 1988) mean annual cycle. The precipitation is averaged over the regions (a) Eastern US (90W-75W, 30N-45N). The plot for the observed precipitation is given by the curve at the top of the figures. The models are arranged alphabetically as in Table 1 with #1 being the BMRC model and #30 being the YONU model. The dark shading indicates the model precipitation exceeds the observed value, the light shading indicates that the observations exceed the model estimates. The scale for all the model deviations is given by the indicator to the right of model #30.

b

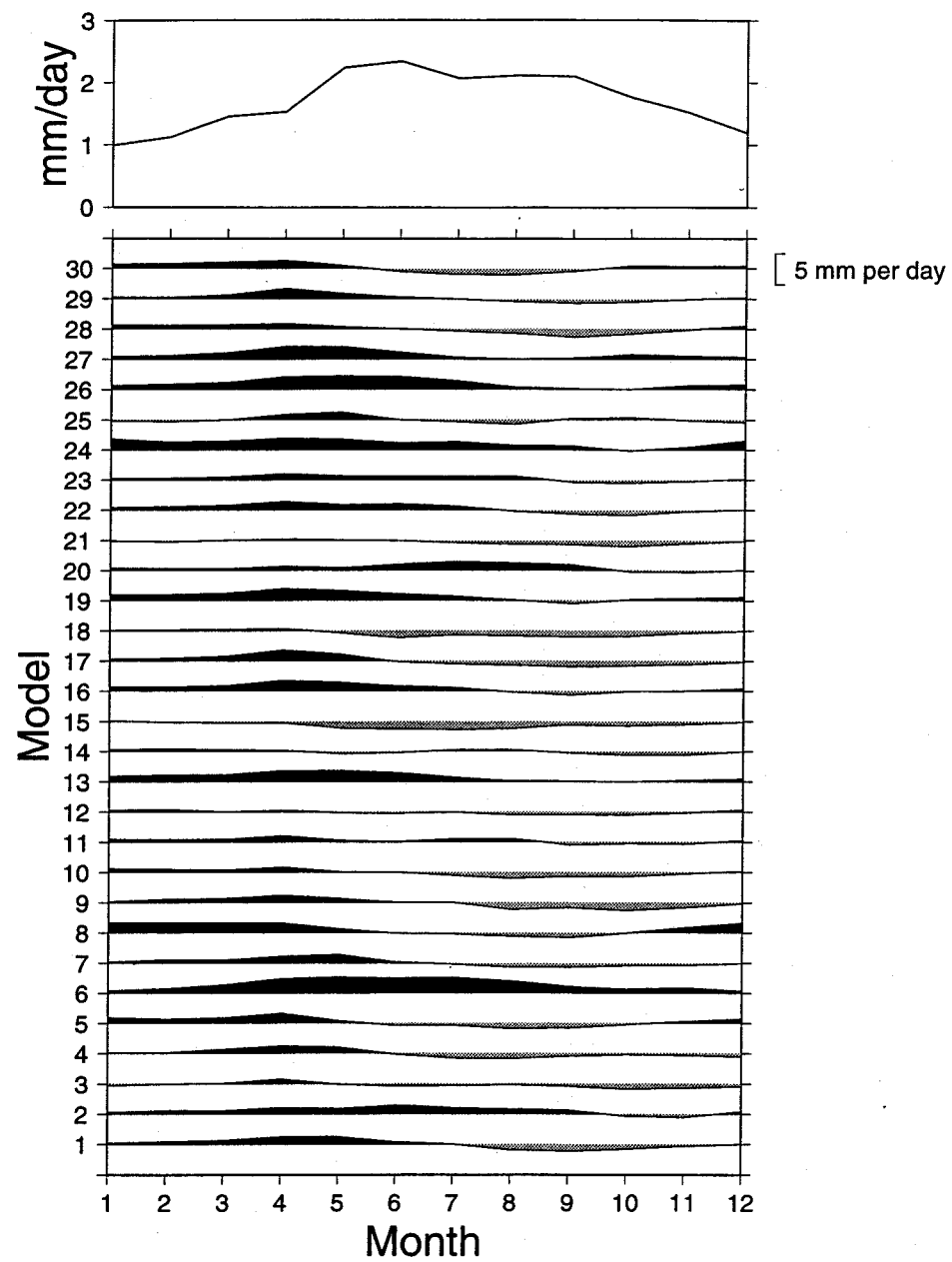


Figure 3(b) as in (a) except for central US (110W-90W , 30N-50N).

C

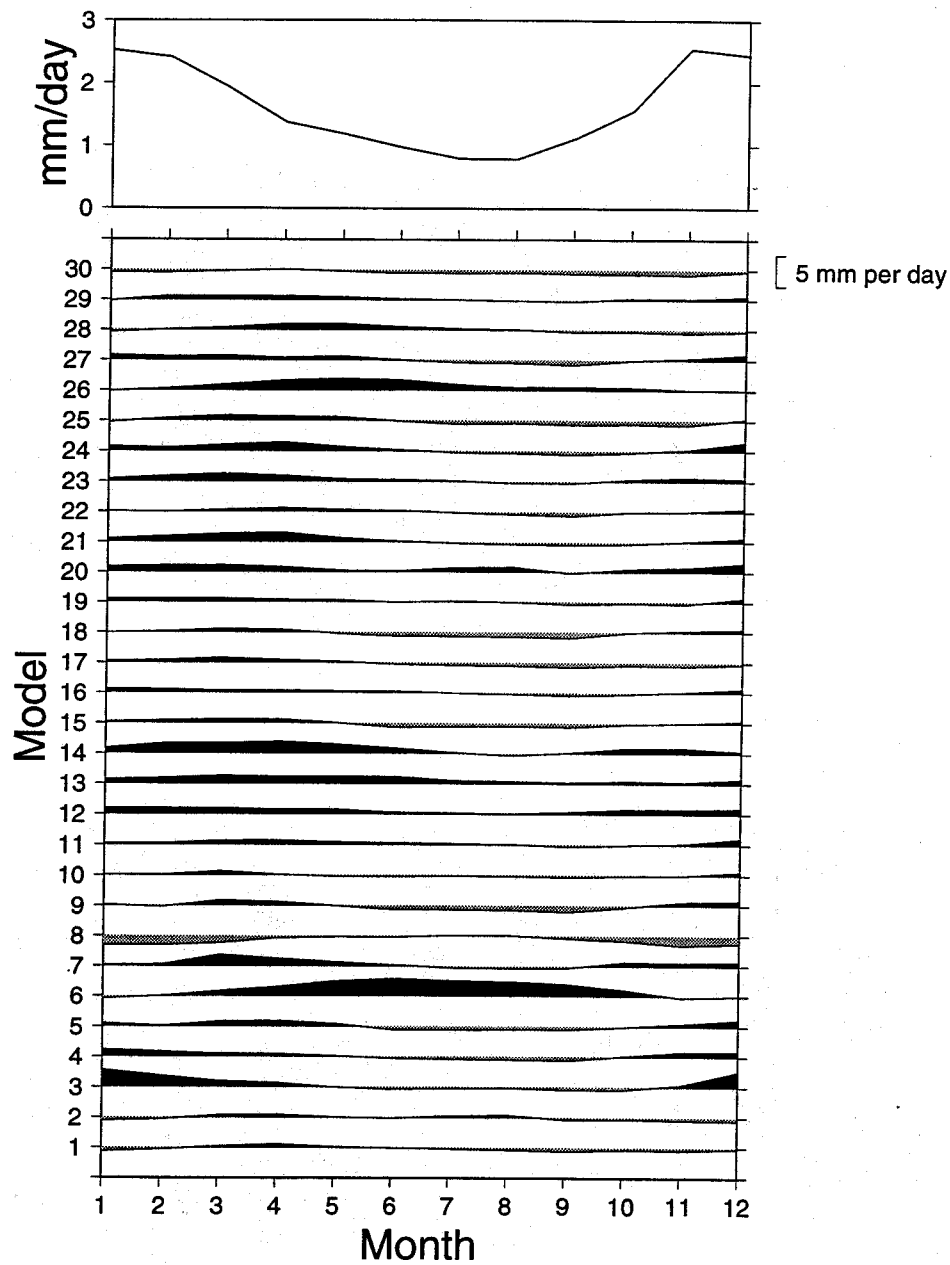
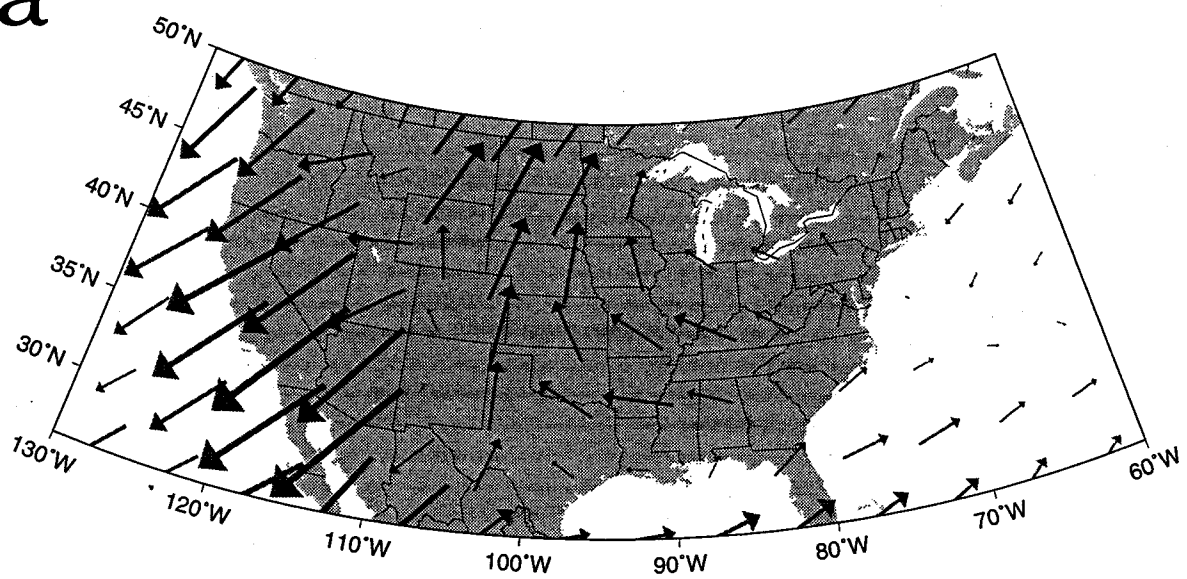


Figure 3(c) as in (a) except for western US (130W-110W, 30N-50N).

a



b

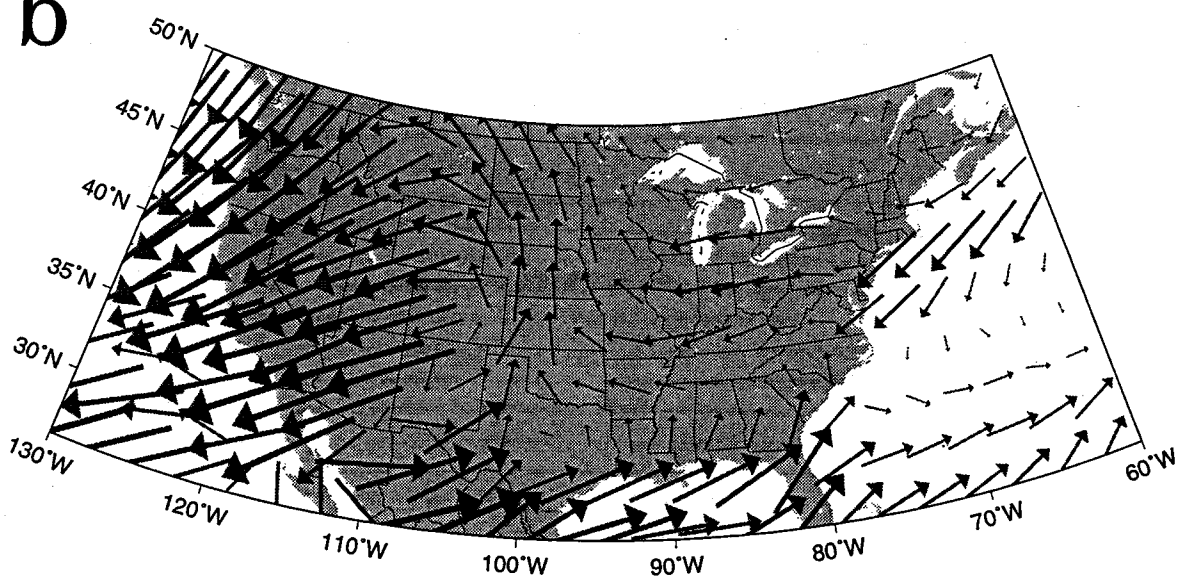


Figure 4. (a) As in Fig. 1 except for the GISS model. (b) As in Fig. 1 except for the MPI model.

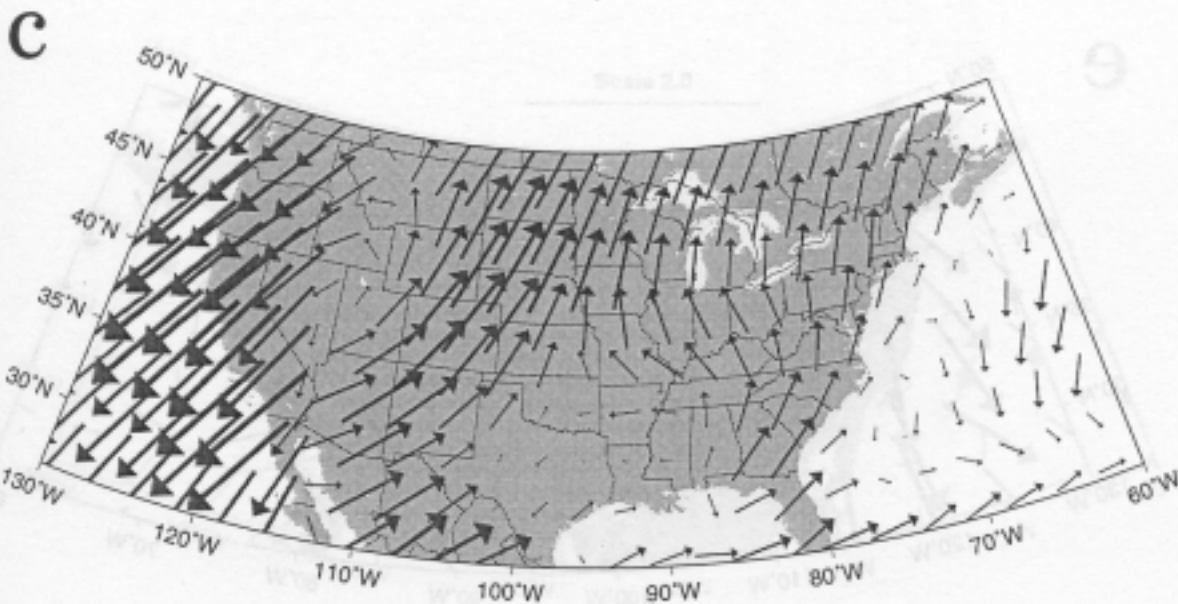


Figure 4. (c) As in Fig. 1 except for the NCAR model .(d) As in Fig. 1 except for the JMA model.

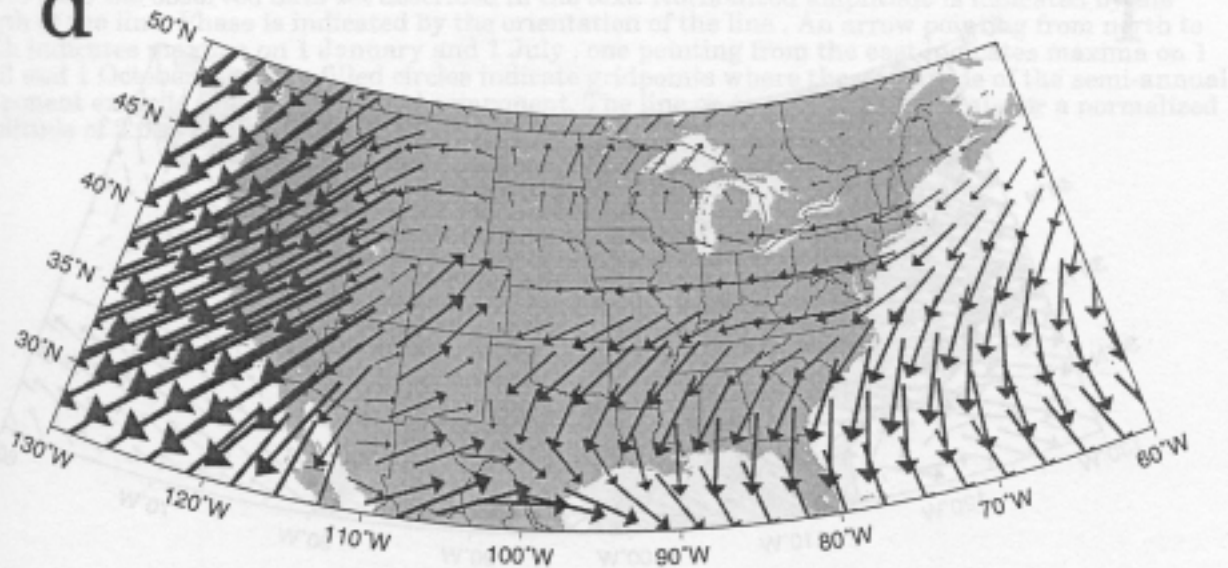


Figure 4. (c) As in Fig. 1 except for the NCAR model .(d) As in Fig. 1 except for the JMA model.

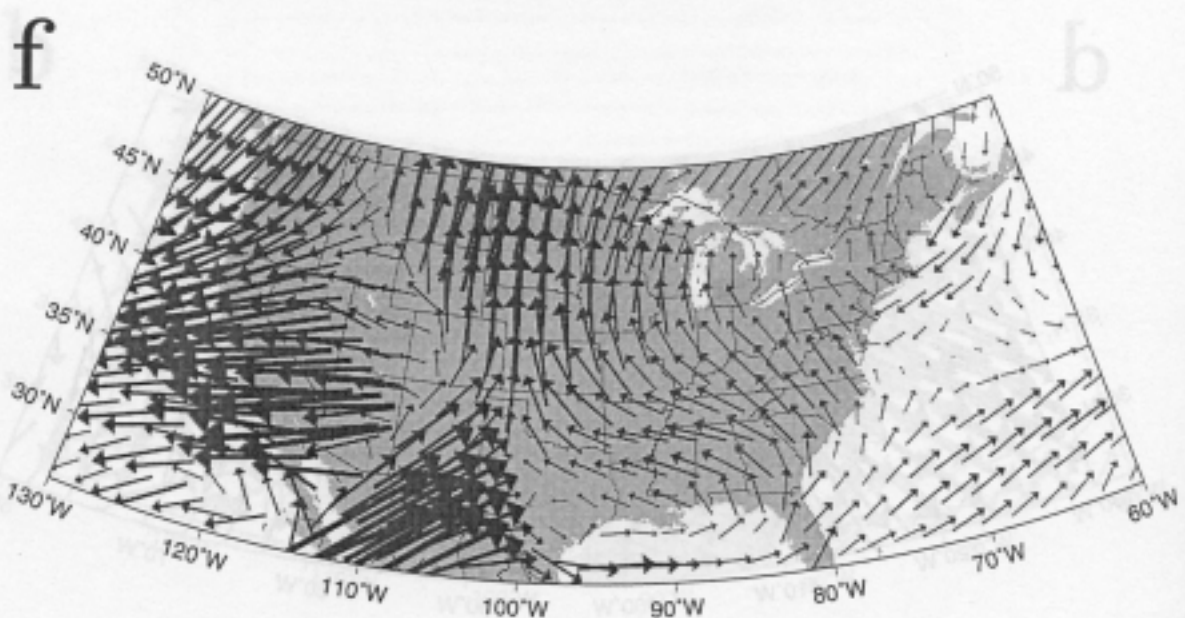
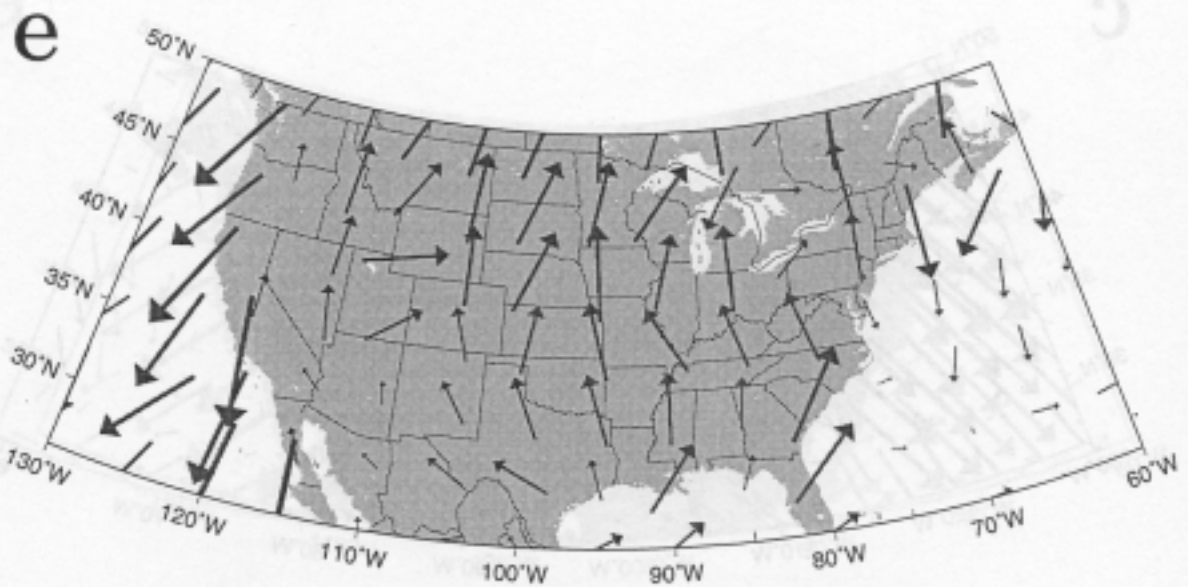


Figure 4. (e) As in Fig. 1 except for the CSU model. (f) As in Fig. 1 except for the RPN model.

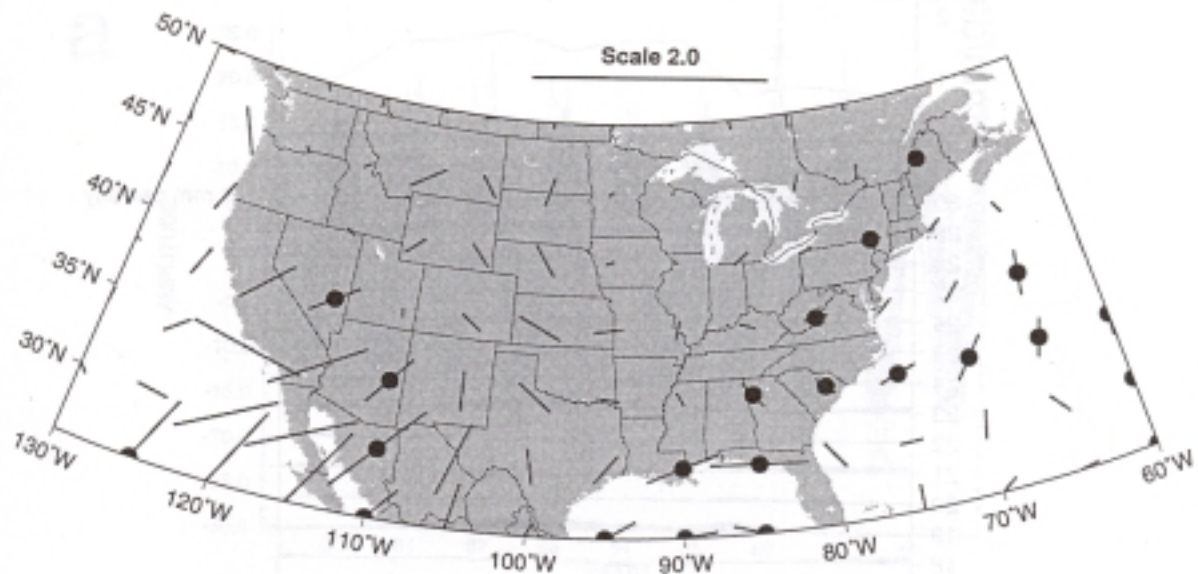


Figure 5. Normalized amplitude and phase of the semi-annual cycle in precipitation over the United States from the observed data set described in the text. Normalized amplitude is indicated by the length of the line. Phase is indicated by the orientation of the line. An arrow pointing from north to south indicates maxima on 1 January and 1 July, one pointing from the east indicates maxima on 1 April and 1 October, etc. The filled circles indicate gridpoints where the amplitude of the semi-annual component exceeds that of the annual component. The line on top provides the scale for a normalized amplitude of 2.0.

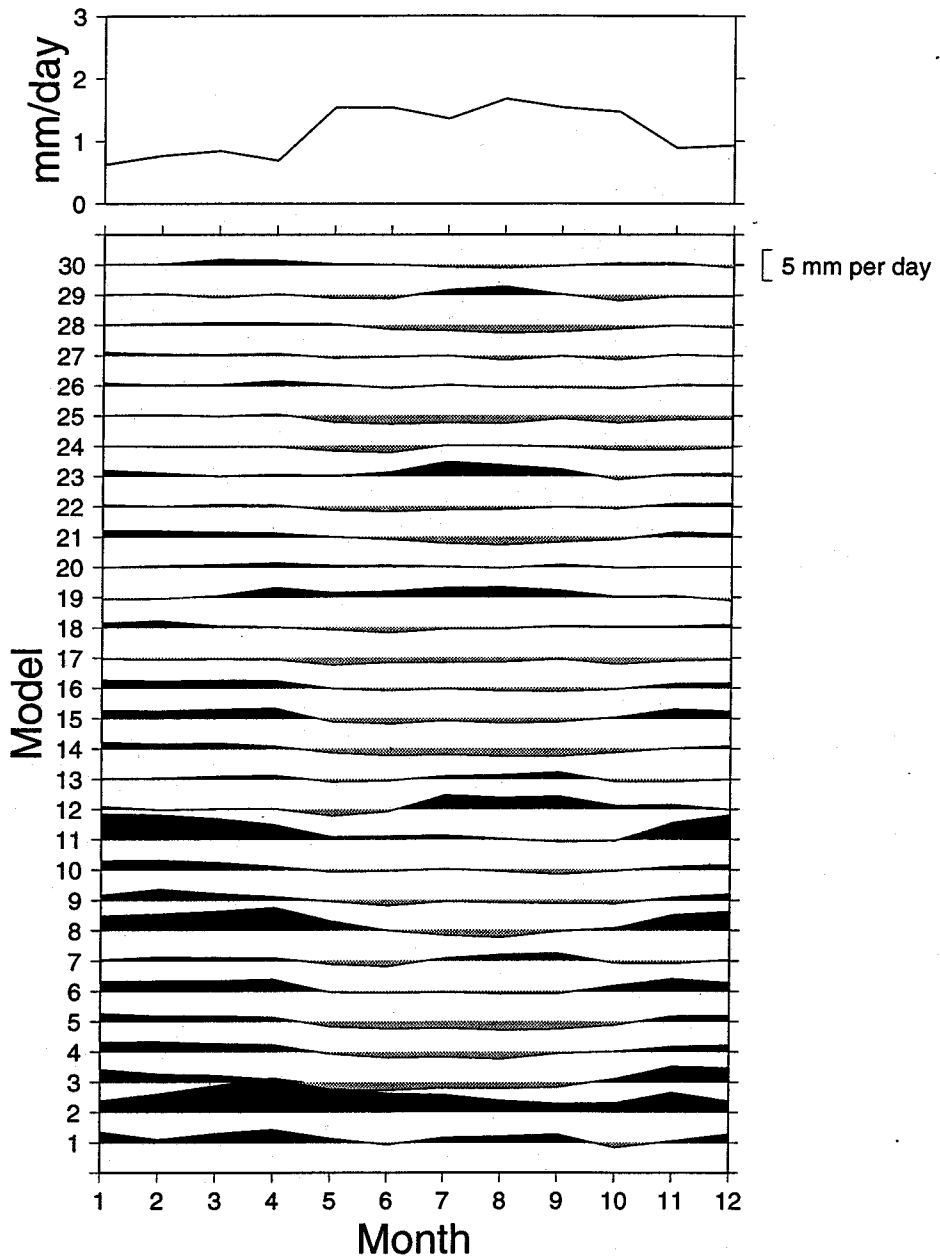
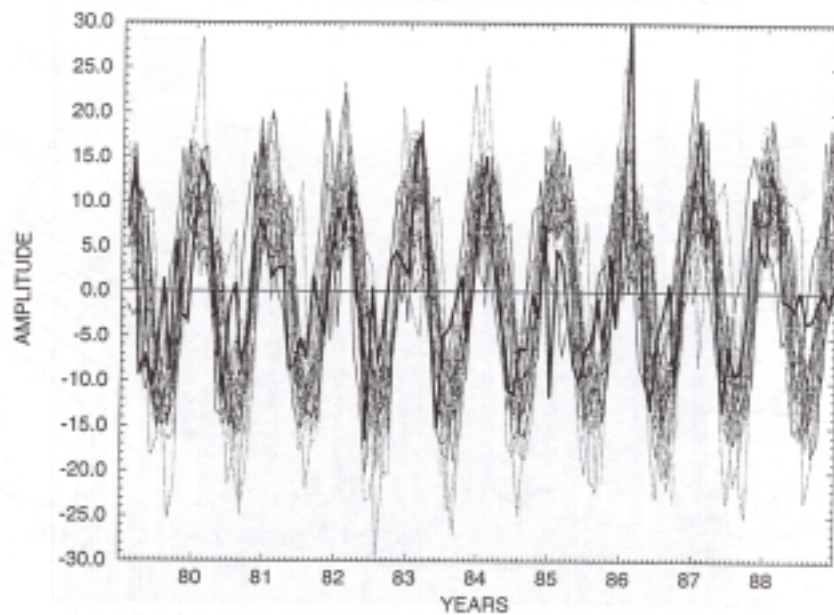


Figure 6. Deviations of the areal averaged precipitation of the AMIP models from the observations over the 10 year (1979 to 1988) mean annual cycle averaged over the region centered over Arizona (29N-36N, 111W-102W). The plot for the observed precipitation is given by the curve at the top of the figures. The models are arranged by horizontal resolution with #1 being the coarsest resolution and #30 being the finest. The dark shading indicates the model precipitation exceeds the observed value, the light shading indicates that the observations exceed the model estimates. The scale for all the model deviations is given by the indicator to the right of model #30.

a



b

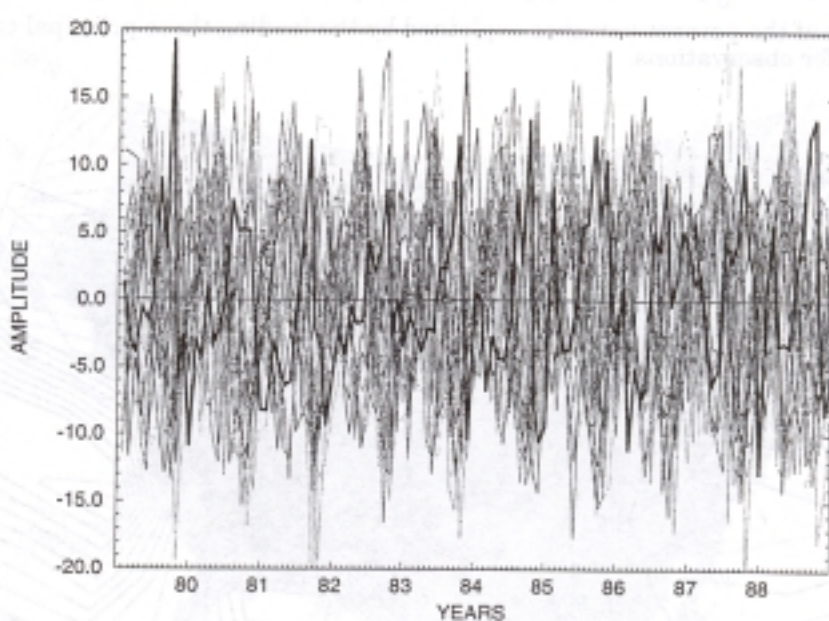


Figure 7. (a) Time series of leading principal component for the AMIP models and for the observed data set. The observed curve is the thick solid line. (b) As in (a) except for the second principal component.

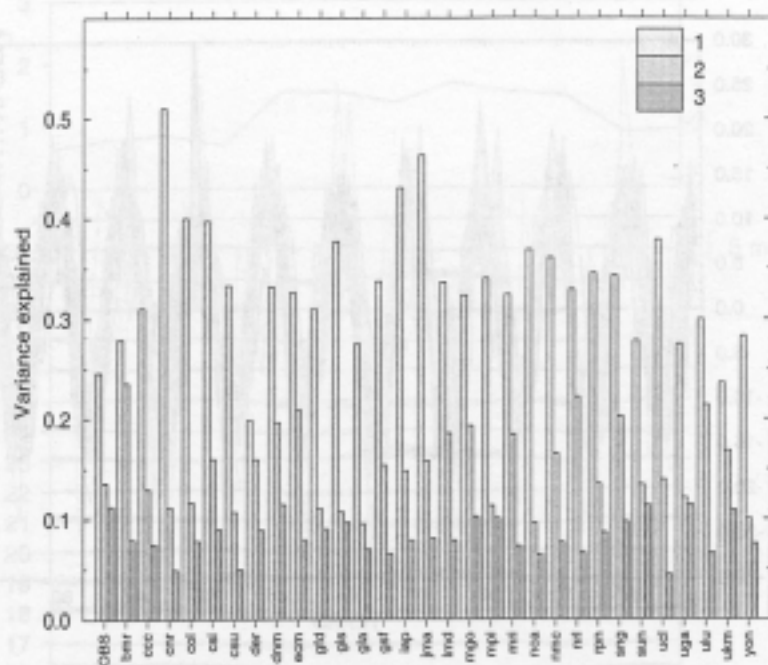


Figure 8. Bar chart of the percent variance explained by the leading three principal components for the AMIP models and for observations.

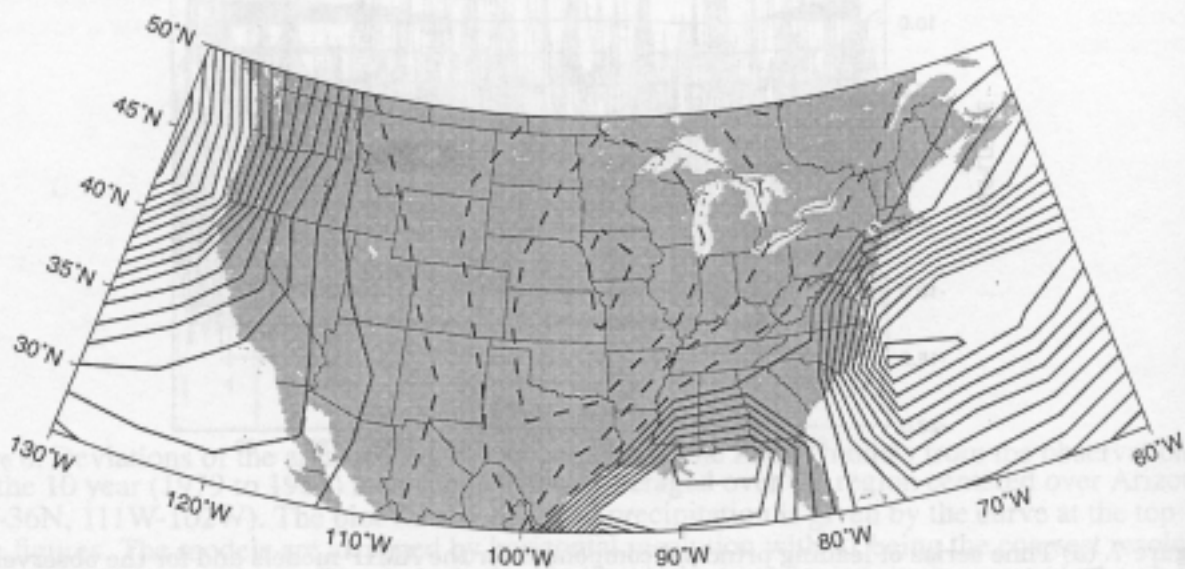
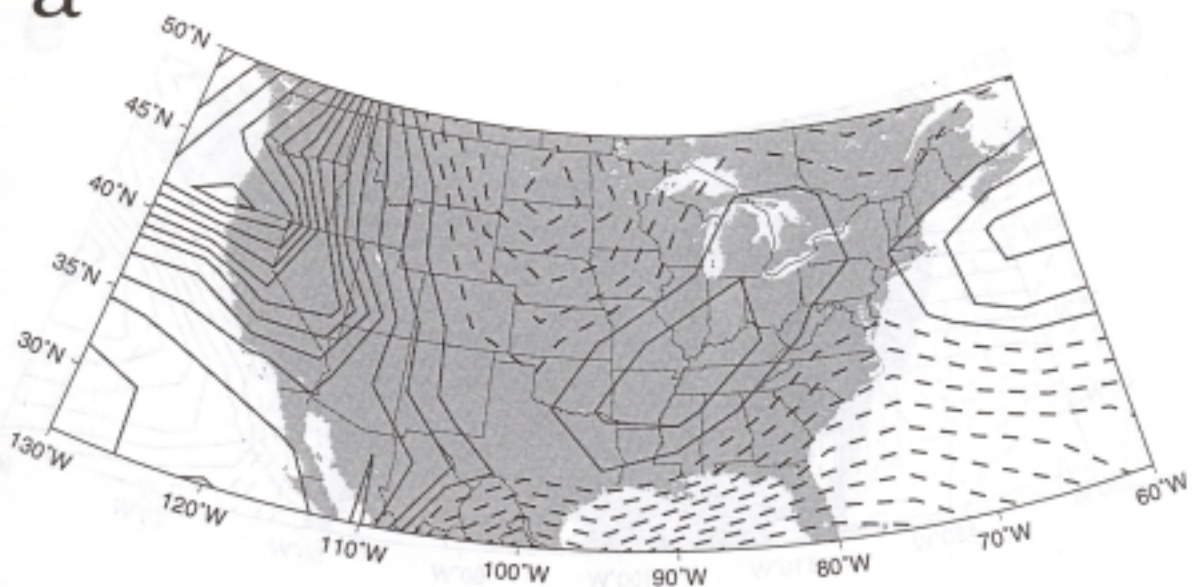


Figure 9. Contour plot of the amplitude of the leading principal vector for the observed precipitation data. The solid lines are zero and positive values, the dashed lines indicate negative values. The contour interval is 0.025.

a



b

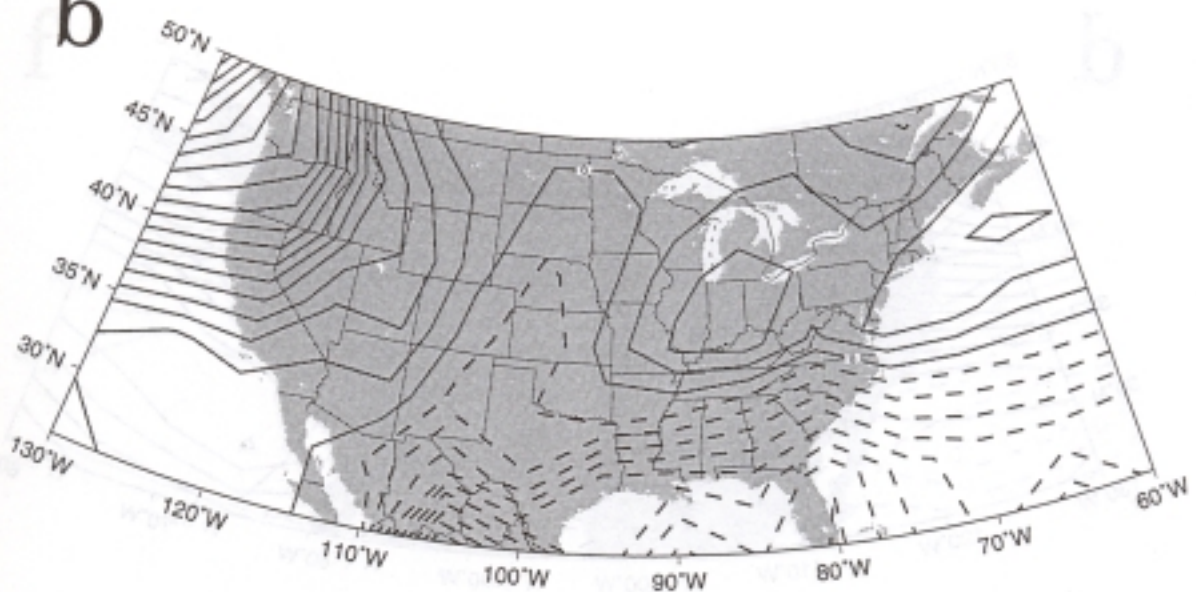


Figure 10. (a) Contour plot of the leading principal vector for the GISS model precipitation data. The solid lines are zero and positive values, the dashed lines indicate negative values. The contour interval is 0.025. (b) As in (a) except for the MPI model.

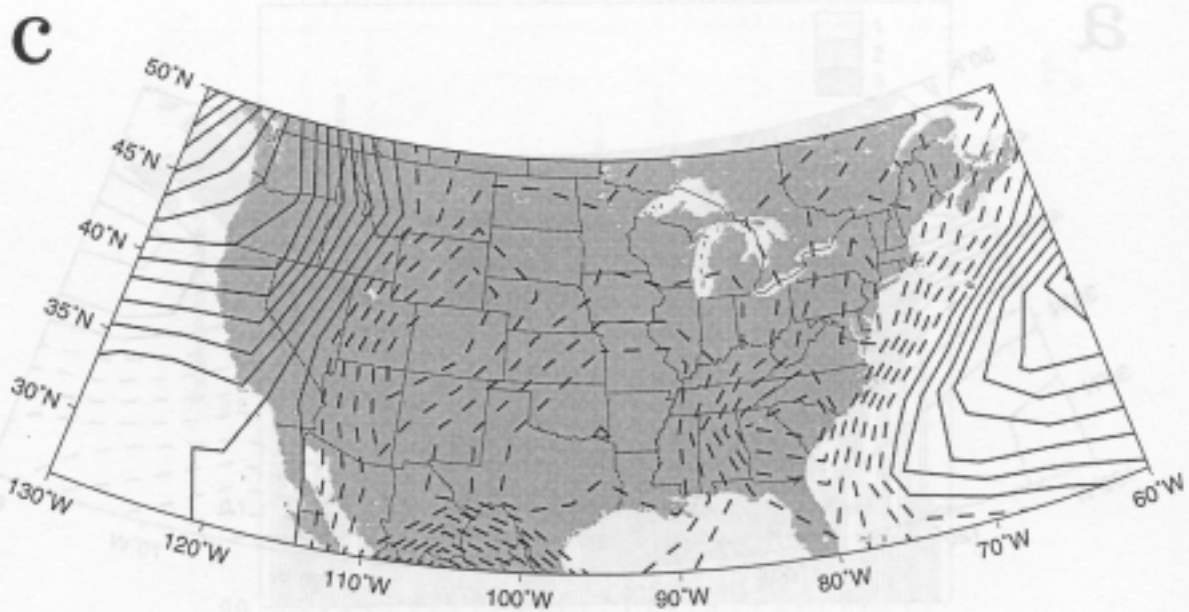


Figure 10. (c) As in (a) except for the NCAR model. (d) As in (a) except for the JMA model.

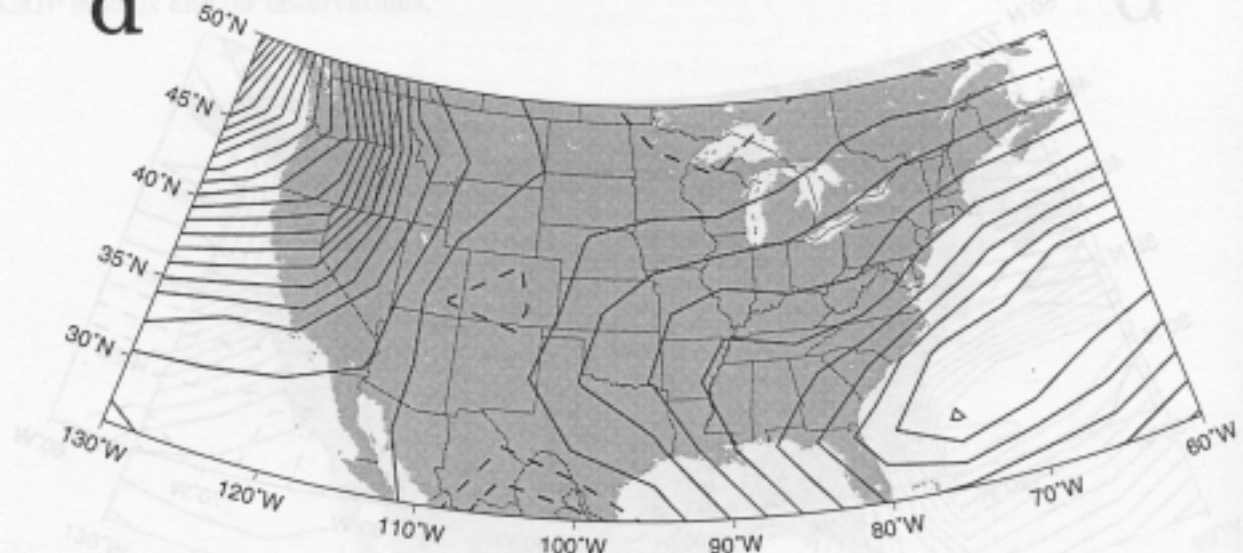
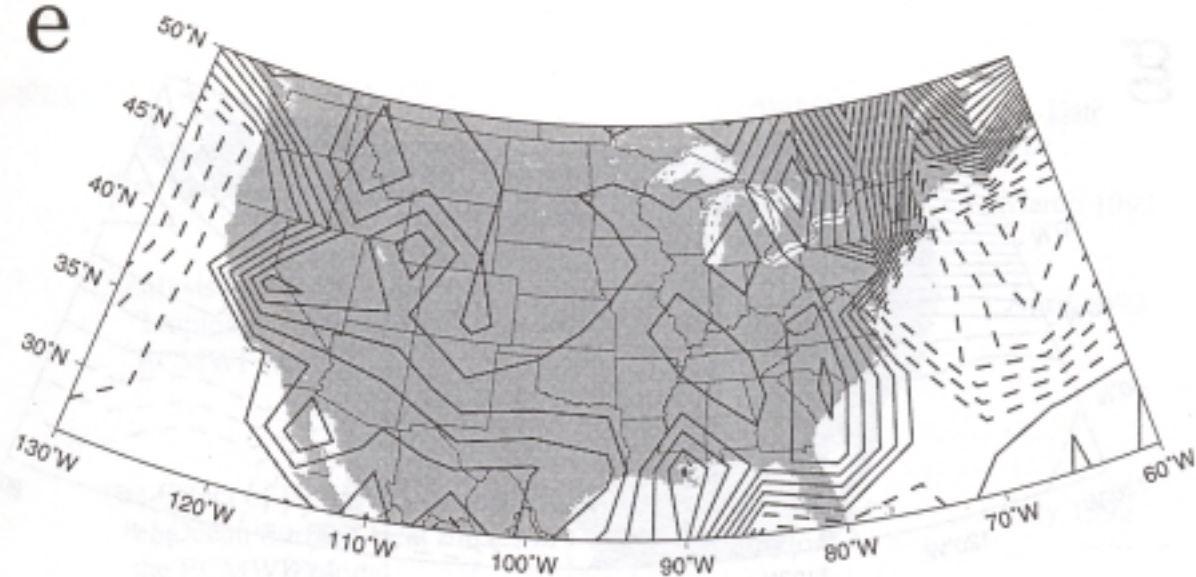


Figure 10. (c) As in (a) except for the NCAR model. (d) As in (a) except for the JMA model.

Figure 9. Contour plot of the amplitude of the leading principal vector for the observed precipitation data. The solid lines are zero and positive values, the dashed lines indicate negative values. The contour interval is 0.025.

e



f

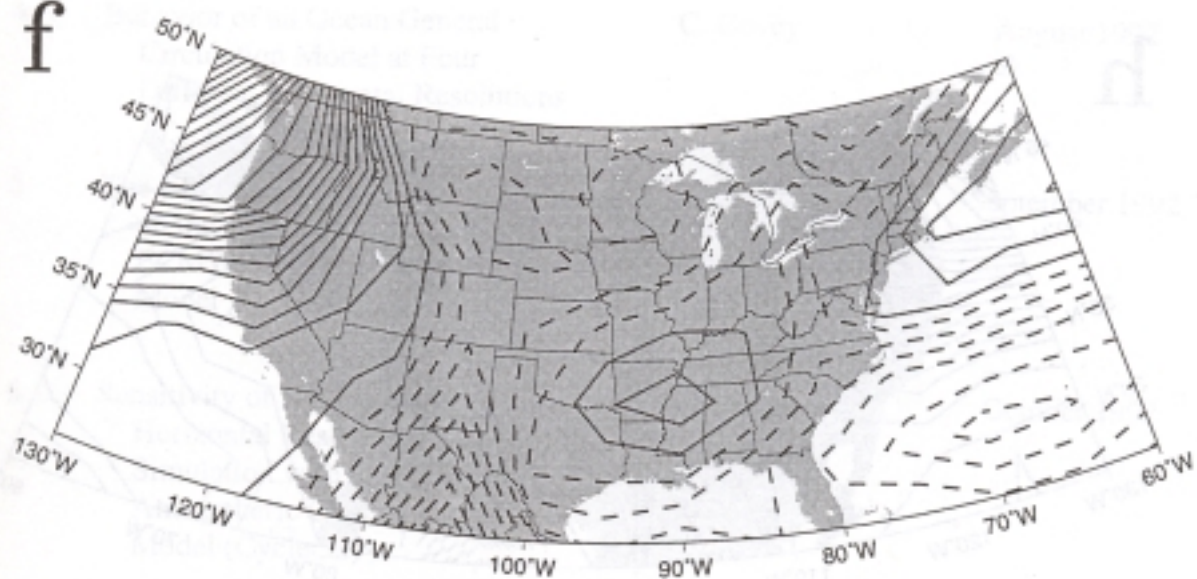


Figure 10. (e) As in (a) except for the CSU model. (f) As in (a) except for the RPN model

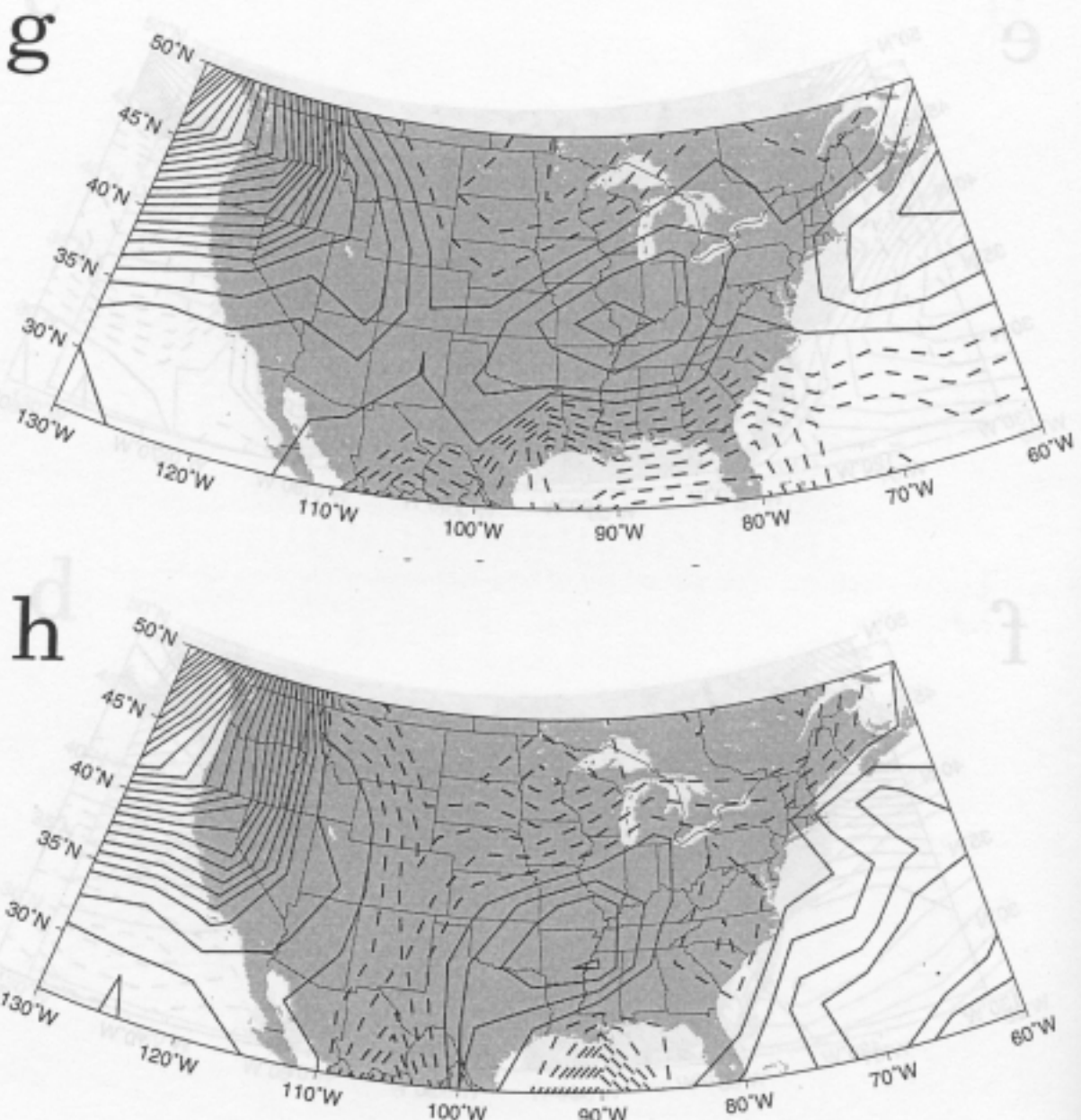


Figure 10. (g) As in (a) except for the NCAR model. (h) As in (a) except for the GFDL model.
Isobars: 1000 mb and 980 mb (a) and (g); Isobars: 1000 mb and 980 mb (h); (a) -01 and (h)

Figure 10. (g) As in (a) except for the ECMWF model. (h) As in (a) except for the UGAMP model.